Int J Adv Manuf Technol (2017) 92:3051–3061
DOI 10.1007/s00170-017-0410-2

ORIGINAL ARTICLE

Laser additive manufactured Ti–6Al–4V alloy: tribology and corrosion studies

P. Chandramohan[1] · **Shepherd Bhero**[1] · **Babatunde Abiodun Obadele**[2] · **Peter Apata Olubambi**[2]

Received: 6 December 2016 / Accepted: 7 April 2017 / Published online: 18 April 2017

Abstract The effect of heat treatments (HT) on wear and corrosion of direct metal laser-sintered Ti–6Al–4V specimens have been studied. Rectangular parts were built in vertical (VB) and horizontal (HB) directions and heat treated above β transus and below β transus with different cooling rate. Rotary wear tests have been carried out under varying loads of 5 N, 15 N and 25 N at 25 m/s. Corrosion behaviour were analysed in 1 M H_2SO_4,1 M HCl and 3.5% NaCl solutions. Wear volume loss of both HB and VB are less in specimens subjected to HT 2 than in HT1 which is attributed to more grain refinement. Presence of compact oxide debris on the surface of HT 2-VB specimen could have contributed to the low wear volume. A sharp positive difference could be observed in OCP immersed in 1 M H_2SO_4solution from −0.6 V (as-sintered) to 0.069 V (HT 1-HB) and 0.089 V (HT 2-HB). I*corr* value in 1 M H_2SO_4 improved after both the heat treatments from 17.450 μA/cm^2 to 1.470 and 0.152 11 μA/cm^2, respectively. Generally, heat-treated specimens (both horizontal and vertical) show better corrosion resistance than the as-sintered specimens in all the three media.

Keywords Heat treatment · Hardness · Microstructure · Wear · Corrosion

✉ P. Chandramohan
pcmohu@yahoo.co.in

[1] Department of Metallurgy, University of Johannesburg, Johannesburg 2028, South Africa

[2] Department of Chemical Engineering, University of Johannesburg, Johannesburg 2028, South Africa

1 Introduction

Additive manufacturing (AM) is used to develop quick prototypes using digital means and hence it shortens the manufacturing period of end product [1]. Application of Ti–6Al–4V lies in aircraft sector and in biomedical implants due to its high specific strength, corrosion resistance and biocompatibility. In recent period, it has also extended into automobile sector to satisfy the requirements like fuel efficiency through weight reduction, greenhouse gases and absorption of energy during crash [2].

Ti–6Al–4V alloy in as-sintered condition develops β grains in columnar form that grow epitaxially from the base. The α phase in the grain boundaries of β is the typical microstructure and subsequent heat treatment coarsens the α phase thus reducing plasticity. Solution treated (4 h at 1223 K, air cooled and aged for 2 h at 873 K followed by air cooling) Ti–6Al–4V specimens failed due to shear upon quasi static compression but improves yield and compressive strength, sacrificing plasticity [3]. Ti–6Al–4V rolled alloy annealed in α + β phase region give in higher super plastic elongation [4].

Process parameters like powder flow rate, layer thickness, scan speed, laser intensity and spot size determines the surface roughness of the material to a larger extent. They also claim that sloping angle have some influence of the surface roughness. Surface roughness of less than 9 μm can be attained by tilting the parts between 10 and 20 degrees relative to the substrate [5]. Alcisto et al. report a relatively inferior surface finish in the as-sintered Ti–6Al–4V alloy [6] and even post heat treatment studies do not improve it [7]. In general, focused research is needed to fix the appropriate process parameters for specific components based on its profile and functionality.

Corrosion behaviour of Ti–6Al–4V alloy have been studied by various researchers in different solutions based on its field of application.

Ti–6Al–4V alloy was tested for its corrosion resistance in NaCl and HCl solutions. It is found to behave inferior in NaCl solution and better in its XY-plane of HCl solution. Lesser α′ and more β-Tiwere the recommended microstructure [8, 9]. Heat treated (1066 °C with furnace-cooling) alloy analysed for corrosion in a 0.5-M H_2SO_4 and 1-M HCl solution mix reports selective dissolution of α phase with increase in step height between α and β as a result of increased timing. Both α and β phases get coarsened without change in its volume fraction [10]. Ti–6Al–4V alloy, tested for corrosion rate in Ringer's solution (simulated body fluid) displayed an I_{Corr} of 2.28 μA/cm^2 and E_{Corr} of −72.5 mV that reduces to an I_{Corr} value of 1.50 μA/cm^2 and E_{Corr} value of −248 mV after coating with hydroxyl apatite and 10% SiO_2 [11]. A comparative study on corrosion of α′ Ti–6Al–4V and α + β Ti–6Al–4V in Ringer's solution favours α′ Ti–6Al–4V due to formation of better oxide protection layer. It has also out performed in its wear resistance due to its microstructure and hardness [12]. Ti–6Al–4V alloy coated with nitride at 36 °C Ringer's solution temperature increase the corrosion resistance with increase in TiN phase content [13]. A fretting corrosion study carried out on Ti–6Al–4V alloy in artificial saliva shows that the fretted locations wear volume increase from 3.26×10^{12} nm^3 to 9.87×10^{12} nm^3 with190ppm of fluoride ions [14].

Dry and wet tribology studies have been attempted in this alloy by various researchers in as-sintered and in heat-treated conditions. Enhancement in wear has been tried through various means like heat treatment, surface treatment, coatings, machining etc. and their wear mechanisms were reported.

SLM produced and heat treated (720–740 °C: furnace cooling) Ti–6Al–4V specimens undergoes grain refinement and hence hardness reduces witnessing lowest wear rate due to protective tribo-oxide formation [15]. In the dry sliding wear tests conducted between 20 and 400 °C, adhesive and abrasive wear occurred till 200 °C and the least wear rate is recorded at 400 °C which is attributed to the protection of tribo-oxides [16]. Above β transus treated and water quenched specimen offered lowest wear loss in Ringer's solution due to the formation of hard martensite in its microstructure. It is also found that material loss increases as the sliding speed and load increases. Wear mechanism in above β transus treated is abrasion and in below β transus treated, its transfer layer formation, abrasion and cracking [17]. Lower wear rate is recorded for water quenched specimens from 950 °C than the air cooled and furnace cooled due to its acicular martensitic microstructure and formation of oxide layer [18]. Laser (250 W) surface melting of Ti–6Al–4V alloy alters the microstructure during solidification with more acicular α in β matrix increasing hardness. This improves the wear rate from 6.82×10^{-4} mm^3/Nm to 3.38×10^{-4} mm^3/Nm along with improvement in corrosion resistance due to the formation of passive oxide layers [19]. The dry wear analysis of Ti18 alloy which is similar toTi–6Al–4V has less effect on increase in coefficient of friction (COF) with increase in load from 1 to 3 N. Abrasive wear with ploughs were reported as the main wear mechanism [20]. Lubricated wear analysis carried out with increase in sliding speed decrease the wear rate up to a load of 30 N and ineffectiveness of lubricants may lead to adhesion rather than abrasion [21]. The predominant wear mechanism of ZrO_2 and HA sandblasted Ti–6Al–4V was reported to be delamination [22]. Solid particle erosion wear in Ti–6Al–4V is mainly due to impact velocity rather than its angle, microstructure and erodent size. Still, lamellar microstructure sustains best erosion resistance than the equiaxed and bimodal one. Ploughing is found to be the main mechanism of erosion loss [23]. Micro-abrasive wear tests have been conducted on Ti–6Al–4V dental implant in contact with hydrated silica particles. Wear loss were found to increase linearly up to 0.011mm^3, with increase in the concentration of hydrated silica (¼ wt%). With increase in load in the range of 0.4, 0.8 and 1.2 N, the surface roughness value increase from 0.40 to 1.30 μm [24]. Ti–6A–l4V material studied for its wear behaviour in artificial sea water show unfair results due to the ejection of TiO_2 particles [25]. Higher COF (0.36) was recorded on Ti–6Al–4V tested in artificial saliva at 37 °C [26]. Oxidation treatment carried out in Ti–6Al–4V implant at 700 °C for 1 h forms hard oxide layer which is of high electrochemical stability and friction challenging while subjecting to fretting corrosion tests [27]. Salehikahrizsangi et al. have reported abrasive/adhesive wear mechanism in commercial and nanostructured Ti–6Al–4V, but delamination in nanocomposite with Ti–B [28]. Passive current density under phosphate buffered saline solution is reported to be doubled in Ti–6Al–4V after anodization due to oxidation [29].

It is found that previous research works has not focused much on the effect of built direction in direct metal laser sintered (DMLS) Ti–6Al–4V alloy with respect to wear and corrosion. Hence, this research work is dedicated to report the findings of dry rotary wear and corrosion behaviour of horizontal built and vertical built DMLS Ti–6Al–4V specimens.

2 Materials and method

Gas atomized Ti–6Al–4V alloy spherical powder (TLS Technik GmbH & Co. Germany) with an average particle size of 45 μm was used to produce rectangular parts of size 100 × 30 × 15 mm in vertical and horizontal directions as shown in Fig. 1 at Centre for Rapid Prototyping and Manufacturing, Bloemfontein using DMLS technology in EOSINT M270 machine. The set process parameters are 170 W laser power, scanning speed 1400 mm/s, layer thickness 30 μm, laser spot size 140 μm and high purity argon build atmosphere acting as a shield to avoid oxidation of Ti.

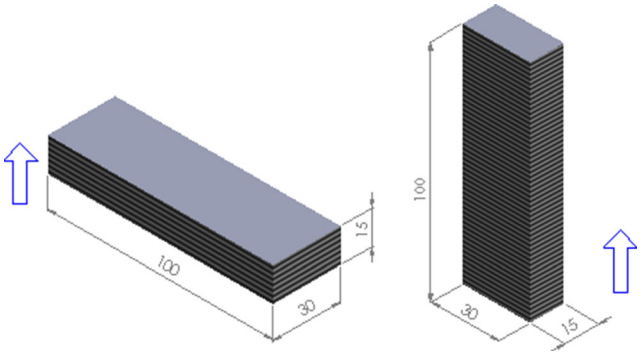

Fig. 1 Rectangular parts produced in horizontal and vertical directions

2.1 Heat treatment

Using horizontal carbolite tube furnace, heat treatments were done by purging argon gas with the following procedures.

1. Heating to 1100 °C (HT-1) at the rate of 5 °C/min, 1 h holding and the cooling rate was 0.09 °C per second.
2. Heating to 900 °C (HT-2) at the rate of 5 °C/min, 1 h holding, cooled at a rate of 0.09 °C per second followed by heating to 650 °C, 3 h holding and then air cool.

2.2 Tribological studies

Tribological studies were carried out for as-sintered and heat treated specimens by conducting dry sliding rotary wear tests using a tribometer CETR UMT-2 with ball-on-disk configuration under varying loads of 5, 15 and 25 N at a speed of 25 mm/s. The wear volume was calculated using the equation in ref. [30].

2.3 Corrosion test

Open circuit potential and potentiodynamic polarization tests were carried out using Autolab PGSTAT 302 supplied by Metrohm, South Africa. The system is equipped with general purpose electrochemical system (GPES) software used for the Tafel extrapolation. Counter electrode material was chosen as graphite rod, reference electrode as saturated silver/silver chloride (Ag/AgCl) and working electrodes as samples. Scan rate of 2 mV $s^{-1}$was chosen to carry out polarization tests from −0.3 to 0.7 V. Three different media; 1 M H_2SO_4, 1 M HCl and 3.5% NaCl, were used to carry out the tests at a temperature of 20 ± 2 °C.

3 Results and discussions

3.1 Microstructure and microhardness of as-sintered and heat-treated Ti–6Al–4V alloy

The microstructures of as-sintered VB, HT 1-VB and HT 2-VB are shown in Fig. 2.

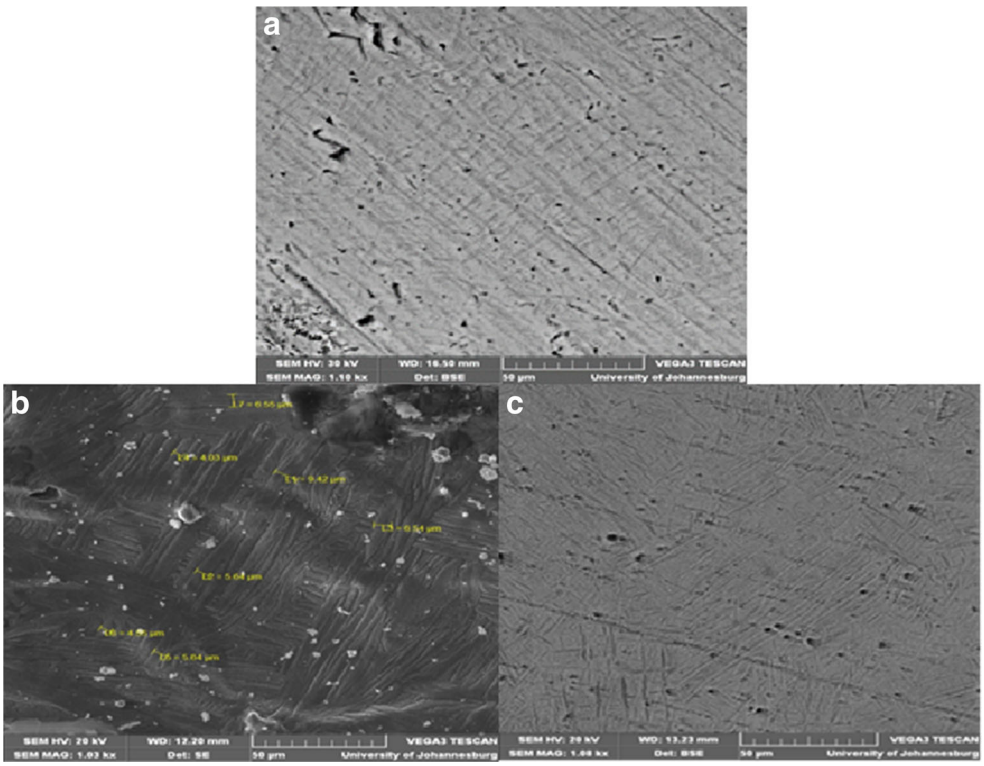

Fig. 2 Microstructures of **a** as-sintered VB, **b** HT 1-VB and **c** HT 2-VB

In the as-sintered microstructure, the presence of martensite (α′) is observed with fine needles of acicular α phase in the β phase matrix. The average grain width in the as-sintered microstructure was about 4 μm. Grain growth from 4.03 to 9.42 μm is noticed after HT 1, since the specimen temperature were elevated above β transus and slow cooled. In HT 2, where the specimens were heated below β transus and air cooled, grain refinement were observed with an average width ranging from 2.03 to 3.89 μm. This observation is not in agreement with the findings of Jin Yao et al., 2016 [3]. Grain refinement is also cross verified by increase in width of XRD peaks of Fig. 4 as per Debye-Scherrer equation [15]. It is also worth mentioning that none of the heat-treated specimen reveals the presence of ά martensite.

Figure 3 shows the microhardness of as-sintered and heat-treated specimens. The microhardness of as-sintered specimens are at higher level due to the presence of ά-martensite and heat treatment reduces the hardness as a whole, probably due to oxide formation as observed in XRD peaks of Fig. 4. Among both the heat treatments, HT 2 specimens show relatively higher hardness due to the observed grain refinement.

3.2 Wear studies

Figure 5 shows the wear performance as a function of wear volume of as-sintered and heat-treated specimens of HB and VB at 5 N, 15 N and 25 N applied loads. It can be noticed that wear volume loss is high in both horizontal and vertical built as-sintered specimens compared to the heat-treated specimens in all the loads applied. This observation is in agreement with the higher microhardness values measured for as-sintered specimens than both the selected heat treatment cycles as noticed in Fig. 3. Generally, the wear volume loss of both HB and VB are less in specimens subjected to HT 2 than in HT1 which is attributed to more grain refinement as evidenced in Fig. 2. More specifically, HT 2-VB recorded the least wear volume. An increase in volume loss was also observed as the load increases from 5 N to 25 N which suggest a gradual transformation from mild wear to severe wear. Similar observation has been reported by Cui et al., 2012 [16].

Figure 6 shows the wear scar of as-sintered and heat-treated specimens under an applied load of 25 N. Parallel ploughs and continuous grooves in the rotary direction can be noticed in all the specimens typical of abrasive wear and adhesive wear mechanism. These images are similar to the reported work of Qiulin Niu et al., 2014 [20] and Obadele et al., 2015 [31]. The presence of compact oxide debris on the surface of HT 2-VB as confirmed from the EDS analysis in Fig. 7 could have contributed to the low wear volume. Compact oxide debris has a lubricating effect on the worn surface and as such could reduce the wear of the material.

3.3 Corrosion studies

The open circuit potential (OCP) curves vs. time of immersion in 1 M H_2SO_4,1 M HCl and 3.5% NaCl solutions for as-sintered HB, HT 1-HB, HT 2-HB, as-sintered VB, HT 1-VB and HT 2-VB are presented in Figs. 8 and 9.

At the end of immersion of HT 1-HB (see Fig. 8b) for 2 h, the OCP in all the three media were about 0.069, −0.089 and −0.28 V, respectively. Generally, a rapid increase in potential was recorded upon immersion in all the three media. It could be observed that on immersion in 1 M H_2SO_4, the OCP increases sharply in the first 600 s and thereafter to more steady noble values without any fluctuations suggesting a passive film formation on the surface of HT 1-HB which is of a quite stable nature. On the other hand, some fluctuations were observed while immersion in both 1 M HCl and 3.5% NaCl solutions. For immersion in 1 M HCl, the OCP increases abruptly in the first 350 s and slight fluctuations were recorded

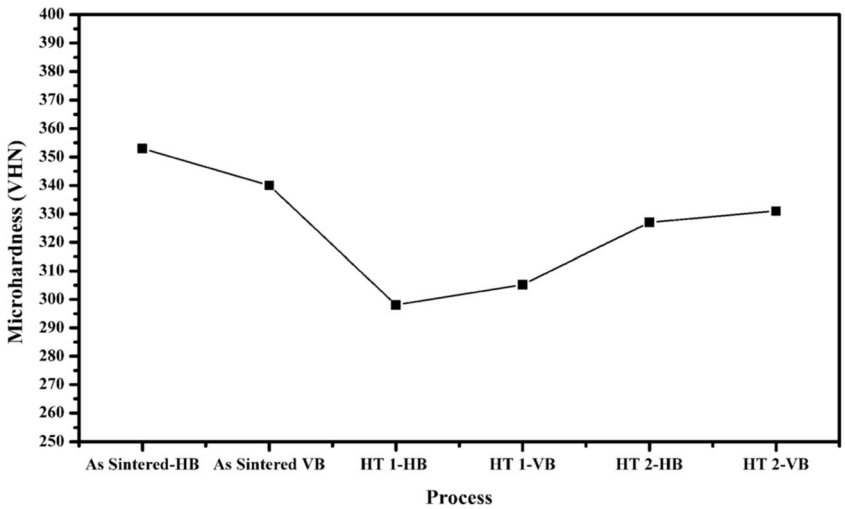

Fig. 3 Microhardness of as-sintered and heat-treated specimens

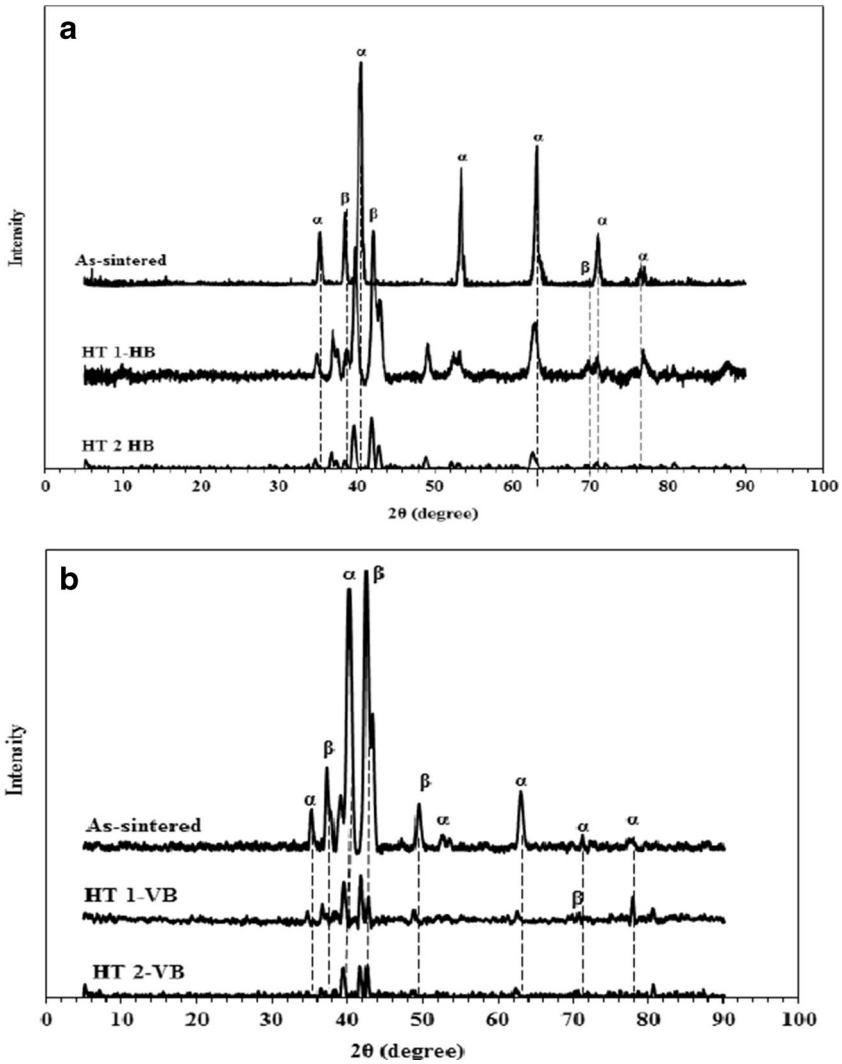

Fig. 4 XRD analysis of as-sintered and heat-treated specimens

until 1200 s and then after, a stable OCP was observed. However, OCP in 3.5% NaCl was oscillating throughout the immersion period reaching a slightly stable potential after 5200 s. Generally, a steady increase in these curves indicates

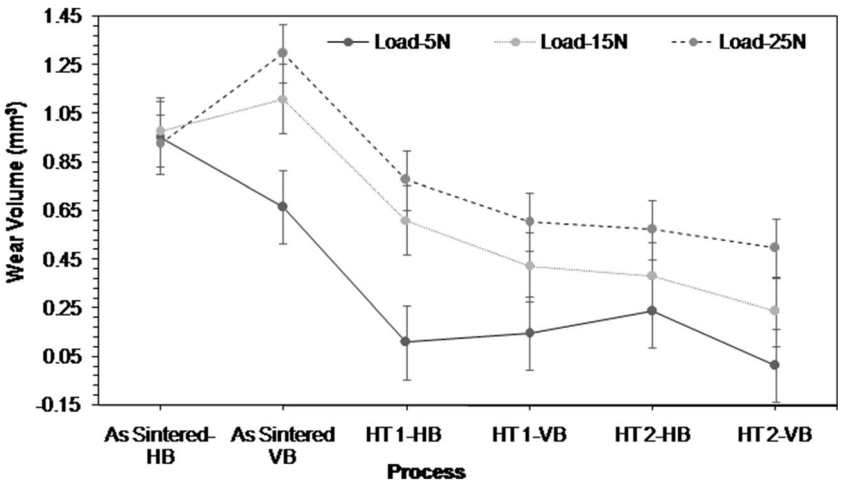

Fig. 5 Wear volume of as-sintered and heat-treated specimens

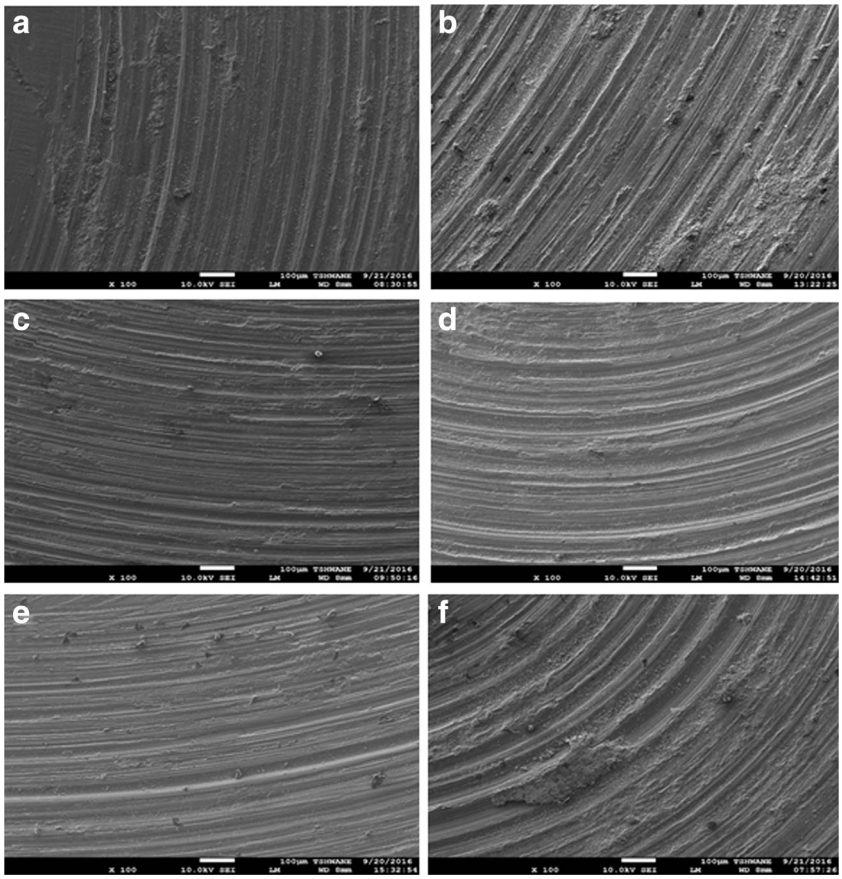

Fig. 6 SEM images of **a** as-sintered HB, **b** as-sintered VB, **c** HT 1-HB, **d** HT 1-VB, **e** HT 2-HB and **f** HT 2-VB worn regions for the applied load of 25 N

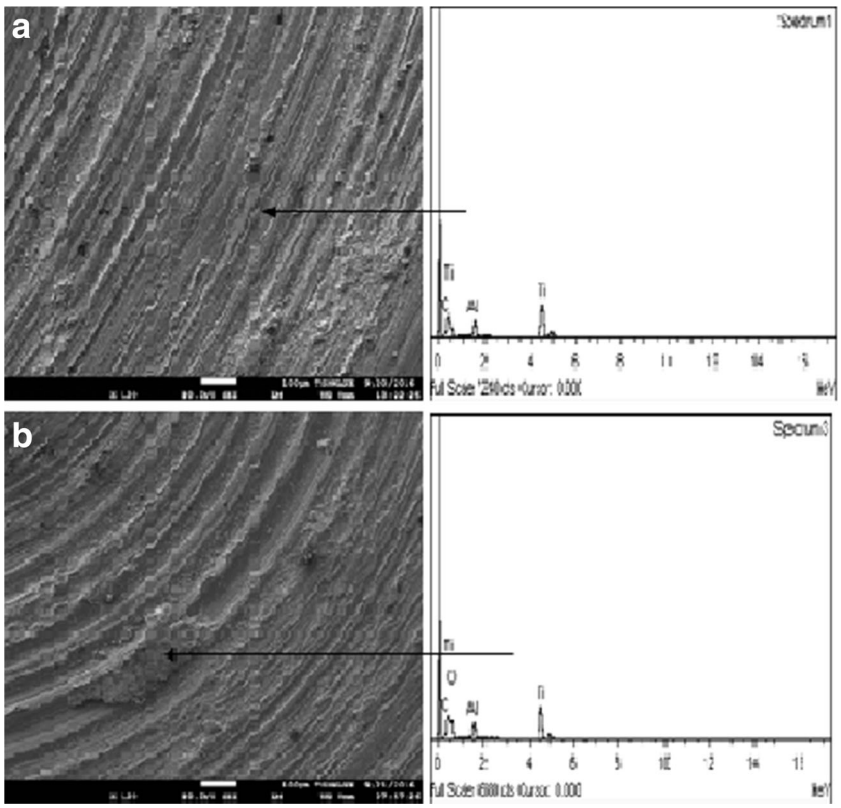

Fig. 7 SEM and EDS of **a** as-sintered VB and **b** HT 2-VB

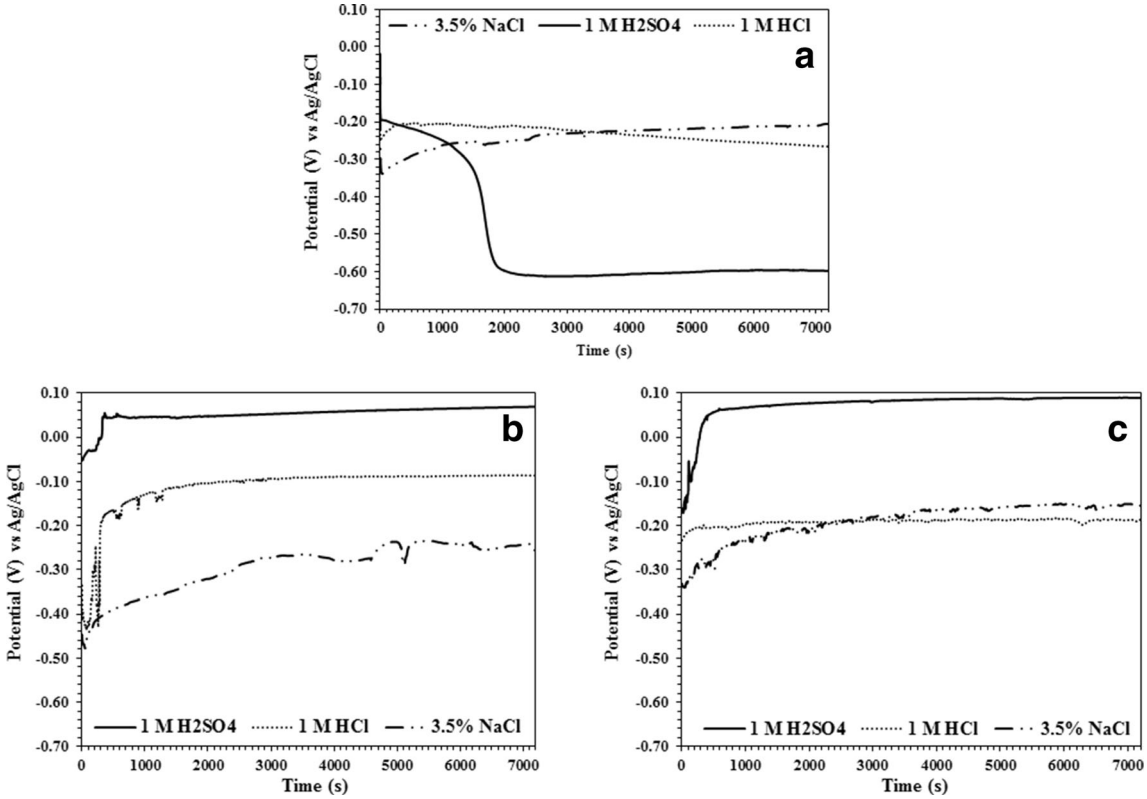

Fig. 8 OCP curves for **a** as-sintered HB, **b** HT 1-HB and **c** HT 2-HB

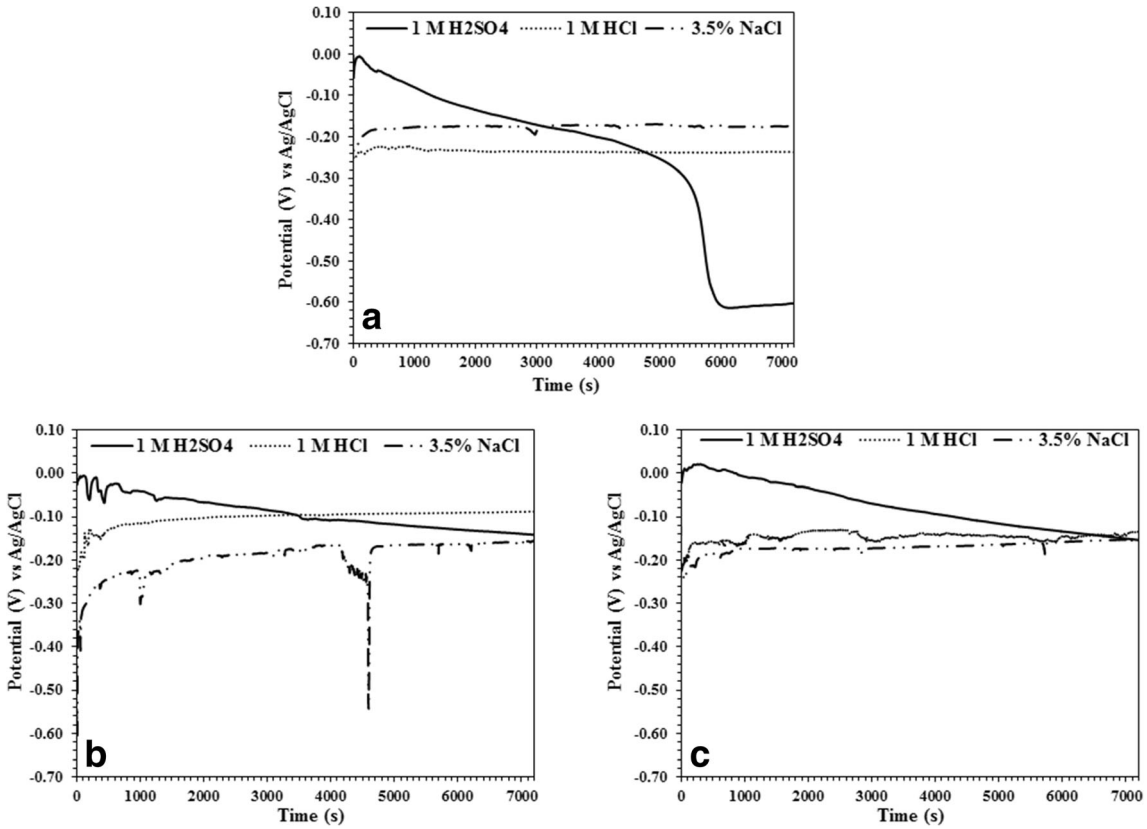

Fig. 9 OCP curves for **a** as-sintered VB, **b** HT 1-VB and **c** HT 2-VB

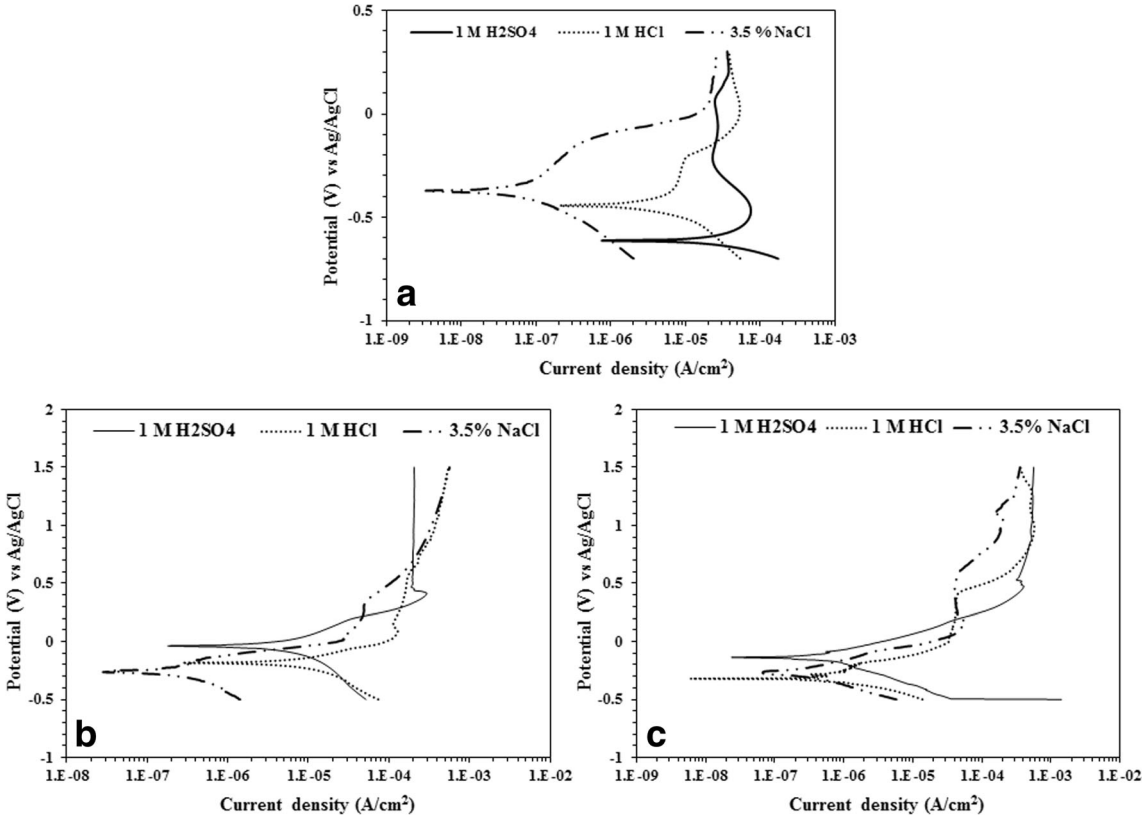

Fig. 10 Polarization curves for OCP curves for **a** as-sintered HB, **b** HT 1-HB and **c** HT 2-HB

the gradual increase in resistance against chemical reactivity. In comparison with as-sintered and HT 1-HB, there is no much improvement in OCP in1 M HCl and 3.5% NaCl solutions whereas a sharp positive difference could be observed from −0.6 V (as-sintered) to 0.069 V (HT 1-HB) in case of 1 M H_2SO_4solution. This shows an improvement of about seven order of magnitude which is due to the existence of high energy acicular ά martensite in as-sintered specimen and its subsequent transformation to β phase after both the heat treatments. Nianwei Dai et al., have also reported similar finding in their work [8, 9].

HT 2-HB sample (see Fig. 8c) upon immersion for 2 h, the OCP in all the three media were about 0.089, −0.19 and −0.15 V, respectively. Upon immersion in 1 M H_2SO_4, the OCP increases to more noble values without much fluctuation and a steady curve was recorded after 400 s. This indicates the formation of an early stable passive film on its surface. Just like in HT 1-HB samples, no substantial improvement in potential could be witnessed after HT-2, but remarkable hike in potential is recorded with 1 M $H_2SO_4$from −0.6 V (as-sintered) to 0.089 V (HT 2-HB).

After 2 h of immersion of HT 1-VB (see Fig. 9b), OCP in all the three media were about −0.14, −0.09 and −0.15 V, respectively. Potential of HT 2-VB (see Fig. 9c) after immersion for 2 h in all the three media were about −0.154, −0.13 and −0.153 V, respectively. Upon immersion of both specimens (HT 1-VB and HT 2-VB) in 1 M H_2SO_4, the OCP slopes down which indicate that passive film formation did not occur throughout immersion in the solutions. There are lot of oscillations conveying very weak formation of stable oxidic layer on its surface, although, a small increase in potential is noticed in both specimens immersed in 1 M HCl and 3.5% NaCl.

Table 1 Current density values for as-sintered HB, HB-HT1 and HB-HT2 in three different solutions

Solutions	E_{corr} (V)	I_{corr} (μA/cm^2)	Corrosion rate (mm/year)
As-sintered HB			
3.5% NaCl	−0.374	0.022	1.97×10^{-4}
1 M HCl	−0.444	1.938	1.70×10^{-2}
1 M H_2SO_4	−0.613	17.450	1.53×10^{-1}
HB-HT1			
3.5% NaCl	−0.26	0.108	3.4×10^{-4}
1 M HCl	−0.19	4.110	1.31×10^{-2}
1 M H_2SO_4	−0.04	1.470	4.67×10^{-3}
HB-HT2			
3.5% NaCl	−0.27	0.105	5.90×10^{-4}
1 M HCl	−0.32	0.714	1.5×10^{-2}
1 M H_2SO_4	−0.14	0.152	8.51×10^{-4}

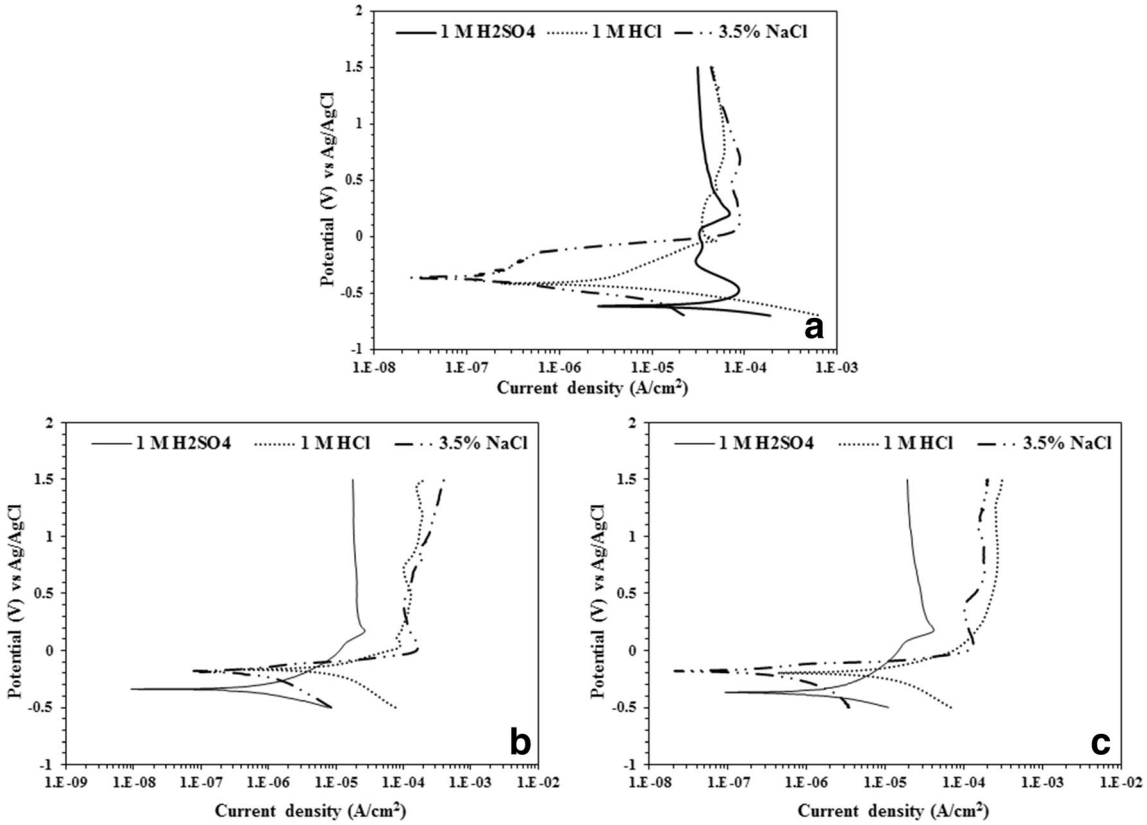

Fig. 11 Polarization curves forOCP curves for **a** as-sintered VB, **b** HT 1-VB and **c** HT 2-VB

Figure 10 clearly displays the polarization curves for as-sintered HB, HT 1-HB and HT 2-HB where the scan rate was set at 2 mV/s in aerated 1 M H_2SO_4, 1 M HCl and 3.5% NaCl solutions. It is clearly observed from Fig. 10b (HT 1-HB sample) that sample immersed in 1 M H_2SO_4 displayed the noblest E*corr* (−0.04 V) followed by 1 M HCl and 3.5% NaCl. An active-passive region was also recorded in both acidic media. In 1 M H_2SO_4, the active-passive region was recorded at higher potential (0.4 V) and high current density (0.0017 μA/cm^2) followed by a stable passivation region, while that of 1 M HCl was recorded at lower potential (0.07 V) and lower current density (0.0015 μA/cm^2) with lower passivation region. The least pitting potential, E*pit*, was observed in sample immersed in 3.5% NaCl, however, no sign of E*pit* in 1 M H_2SO_4. From Table 1 using the Tafel extrapolation method, the corrosion current density, I*corr*, for the samples in the selected media were 1.470, 4.110 and 0.108 μA/cm^2, respectively. This indicates that although, sample immersed in 3.5% NaCl solution had the least E*corr*, it displays the least I*corr* and corrosion rate. This has shown that Ti–6Al–4V has better corrosion resistance in alkaline media when compared to acidic media John A. Mountford [32] reported that titanium does not corrode in almost all-marine applications.

From Fig. 10c (HT 2-HB), it is however observed that sample immersed in 1 M HCl showed no active-passive region with short passivation region and a conspicuous E*pit*. Furthermore, from Table 1, the I*corr* recorded was the highest (0.714 μA/cm^2) with high corrosion rate (1.5 × 10^{-2} mm/year). Generally, there is a marginal improvement in the I*corr* of the heat-treated specimens when compared to as-sintered. From Table 1, the I*corr* for as-sintered sample in 1 M H_2SO_4 is 17.450 μA/cm^2 while heat-treated specimens are 1.470 and 0.152 11 μA/cm^2, respectively.

Table 2 Current density values for as-sintered VB, VB-HT1 and VB-HT2 in three different solutions

As-sintered VB			
3.5% NaCl	−0.369	0.050	4.46×10^{-4}
1 M HCl	−0.420	1.676	1.47×10^{-2}
1 M H_2SO_4	−0.615	17.090	1.50×10^{-1}
VB-HT1			
3.5% NaCl	−0.20	0.266	1.49×10^{-3}
1 M HCl	−0.16	2.360	1.32×10^{-2}
1 M H_2SO_4	−0.34	0.240	1.35×10^{-3}
VB-HT2			
3.5% NaCl	−0.18	0.081	4.56×10^{-4}
1 M HCl	−0.20	2.020	1.13×10^{-2}
1 M H_2SO_4	−0.37	0.789	4.42×10^{-3}

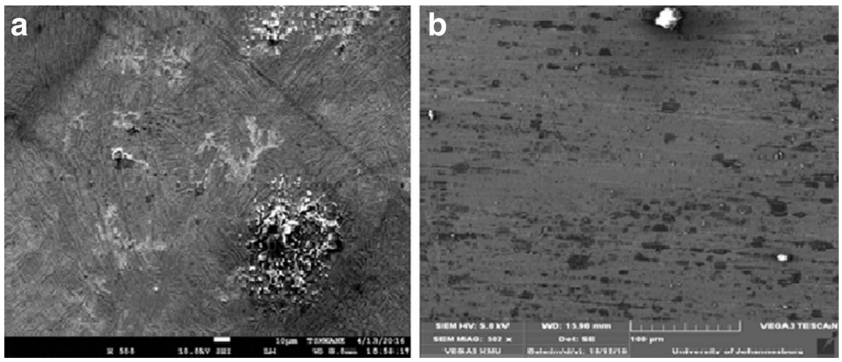

Fig. 12 SEM morphologies of the corroded specimens **a** as-sintered and **b** HT 2-VB in 1 M H_2SO_4 media

The potentiodynamic polarization curves for as-sintered VB, HT 1-VB and HT 2-VB immersed in 1 M H_2SO_4, 1 M HCl and 3.5% NaCl solutions are shown in Fig. 11. From Fig. 11b, it is observed that specimen immersed in 1 M H_2SO_4 displayed the least E*corr* (−0.34 V) and least I*corr* (0.240 μA/cm^2) followed by 3.5% NaCl and 1 M HCl. All the specimens displayed an active-passive region with a steady passive region in 1 M H_2SO_4 and fluctuating passive regions in 1 M HCl and 3.5% NaCl. There are no pitting potential, E*pit*, recorded throughout the experimental test in specimens immersed in any of the solutions. Similar observations were recorded in Fig. 11c (HT 2-VB). When compared with as-sintered specimen, there is an improvement in I*corr* of specimen immersed in 1 M H_2SO_4 as shown in Table 2.

In all, heat-treated specimens (both horizontal and vertical) perform better than the as-sintered specimens in all the three media, more specifically in 1 M H_2SO_4 which is more aggressive than HCl and NaCl environment. Figure 12 clearly displays the SEM morphology of as-sintered VB and HT 2 VB specimen after the corrosion test in 1 M H_2SO_4 with corrosion products present on the specimen surfaces; however, no microcracks were detected. More corrosion products could be observed in the form of cluster on the surface of as-sintered specimen whereas, it is not so in any of the heat-treated specimens.

4 Conclusion

1. Heat treatment has got more influence than build direction in determining wear and corrosion resistance property.
2. Wear volume loss is less in specimens subjected to HT 2 than in HT 1 due to grain refinement.
3. Compact oxide debris on the surface of HT 2-VB backed lowest wear volume.
4. I*corr* in 1 M H_2SO_4 improved after both the heat treatments from 17.450 μA/cm^2 to 1.470 and 0.152 11 μA/cm^2, respectively.
5. Sharp positive difference could be observed from −0.6 V (as-sintered) to 0.069 V (HT 1-HB) and 0.089 V (HT 2-HB), while immersed in 1 M H_2SO_4 solution.
6. Ti–6Al–4V has better corrosion resistance in alkaline media when compared to acidic media

Acknowledgments The authors are grateful to metal casting station, University of Johannesburg, South Africa for funding this research work.

References

1. Sunil Kumar Tiwari Sarang Pande Sanat Agrawal Santosh M. Bobade, (2015), Selection of selective laser sintering materials for different applications, Rapid Prototyping Journal, Vol. 21 Iss 6 pp. 630–648
2. Rao PR (2009) Advances in materials and their applications. New Age International Publishers, New Delhi
3. Jin Yao, Tao Suo, Shuangyin Zhang, Feng Zhao, Hongtao Wang, Jiabin Liu, Yuzeng Chen, Yulong Li, Influence of heat-treatment on the dynamic behaviour of 3D laser deposited Ti–6Al–4V alloy Materials Science & Engineering A 677 (2016) 153–162
4. Indranil Lahiri, Debrupa Lahiri (Mondal), S. Bhargava, Effect of prior β processing on super plasticity of (α+β) thermo mechanically treated Ti–6Al–4V alloy, Materials and manufacturing processes, Vol. 18, No. 4, (2003) 621–635.
5. Krol M, Tanski T (2016) Surface quality research for selective laser melting of Ti-6Al-4V alloy. Arch Metall Mater 61(3):1291–1296
6. Alcisto J, Enriquez A, Garcia H, Hinkson S, Steelman T, Silverman E, Valdovino P, Gigerenzer H, Foyos J, Ogren J, Dorey J, Karg K, McDonald T, Es-Said OS (2001) Tensile properties and microstructures of laser-formed Ti-6Al-4V. J Mater Eng Perform 20:203–212
7. Erhard B, Achim S, Christoph L (2015) Morphology, microstructure, and hardness of titanium (Ti-6Al-4V) blocks deposited by wire-feed additive layer manufacturing (ALM). Journal of Mechanical Behaviour of Biomedical Materials 51:61–73
8. Dai N, Zhang L-C, Zhanga J, Chena Q, Wua M (2016) Corrosion behaviour of selective laser melted Ti-6Al-4V alloy in NaCl solution. Corros Sci 102:484–489
9. Dai N, Zhang L-C, Zhang J, Zhang X, Ni Q, Yang C, Wu M, Yang C (2016) Distinction in corrosion resistance of selective laser melted Ti-6Al-4Valloy on different planes. Corros Sci 111:703–710
10. Chen J-R, Tsai W-T (2011) In situ corrosion monitoring of Ti–6Al–4V alloy inH_2SO_4/HCl mixed solution using electrochemical AFM. Electro chimica Acta 56:1746–1751
11. Gurpreet Singh, Hazoor Singh, Buta Singh Sidhu,Characterization and corrosion resistance of plasma sprayed HA and HA–SiO2 coatings on Ti–6Al–4V, Surface & Coatings Technology 228 (2013) 242–247
12. Cvijovic C-AZ, Mitrovic S, Panic V, M. (2011) Rakin, wear and corrosion behaviour of Ti–13Nb–13Zr and Ti–6Al–4V alloys in simulated physiological solution. Corros Sci 53:796–808

13. Pohrelyuk IM, Fedirko VM, Tkachuk OV, Proskrnyak RV (2013) Corrosionresistance of Ti-6Al-4V alloy with nitride coatings in Ringer's solution. Corros Sci 66:392–398
14. B. Sivakumar, Satendra Kumar, T.S.N. Sankara Narayanan, Fretting corrosion behaviour of Ti–6Al–4V alloy in artificial saliva containing varying concentrations of fluoride ions, Wear 270 (2011) 317–324
15. Y. Zhu, X. Chen, J. Zou, H. Yang, Sliding wear of selective laser melting processed Ti6Al4V under boundary lubrication conditions, Wear, Accepted for publication on.2016.09.20
16. Cui XH, Mao YS, Wei MX, Wang SQ (2012) Wear characteristics of Ti-6Al-4V alloy at 20–400°C. Tribol Trans 55(2):185–190
17. Cvijovic-Alagic Z, Cvijovic S, Mitrovic M, Rakin D, Veljovic M (2010) Babic, Tribological behaviour of orthopaedic Ti-13Nb-13Zr and Ti-6Al-4V alloys. Tribol Lett 40:59–70
18. Ganesh BKC, Ramanaih N, Chandrasekhar Rao PV (October 2012) Dry sliding wear behavior of Ti–6Al–4V implant alloy subjected to various surface treatments. Trans Indian Inst Metals 65(5):425–434
19. Vamsi Krishna Balla, Julie Soderlind, Susmita Bose, Amit Bandyopadhyay, Microstructure, mechanical and wear properties of laser surface melted Ti6Al4V alloy, Journal of the mechanical behaviour of bio medical materials 32 (2014) 335–344.
20. Qiulin NiuXiaohu Zheng Ming Chen Weiwei Ming, (2014),Study on the tribological properties of titanium alloys sliding against WC-Co during the dry friction, Industrial Lubrication and Tribology, Vol. 66 Iss 2 pp. 202–208
21. Mukund Dutt Sharma Rakesh Sehgal, (2014),Experimental study of friction and wear characteristics of titanium alloy (Ti-6Al-4V) under lubricated sliding condition, Industrial Lubrication and Tribology, Vol. 66 Iss 2 pp. 174–183
22. A.B. Hazar Yoruc¸ O. Elkoca, Wear behaviour of Ti6Al4V alloy blasted with zirconia/hydroxyapatite powders, Industrial Lubrication and Tribology, 66/1 (2014) 106–110
23. Sahoo R, Mantry S, Sahoo TK, Mishra S, Jha BB (2013) Effect ofMicrostructural variation on erosion wear behavior of Ti-6Al-4V alloy. Tribol Trans 56(4):555–560
24. Sampaio M, Buciumeanu M, Henriques B, Silva FS, Souza JCM, Gomes JR (2016) Comparison between PEEK and Ti6Al4V concerning micro-scale abrasion wear on dental applications. Journal of the mechanical behaviour of bio medical materials 60: 212–219
25. Vladimir Totolin, Vladimir Pejakovic, Thomas Csanyi, Oliver Hekele, Martin Huber, Manel Rodríguez Ripoll, Surface engineering of Ti6Al4V surfaces for enhanced tribo corrosionperformance in artificial seawater, Materials and Design 104 (2016) 10–18
26. Miguel Sampaio, Mihaela Buciumeanu, Bruno Henriques, Filipe S. Silva, Julio C.*M. Souza*, Jose R. Gomes, Tribocorrosion behaviour ofveneeringbiomedical PEEK toTi6Al4Vstructures, Journal of the mechanical behaviour of bio medical materials, 54 (2016) 123–130
27. Billi F, Onofre E, Ebramzadeh E, Palacios T, Escudero ML, Garcia-Alonso MC (2012) Characterization of modified Ti6Al4V alloy after fretting–corrosion tests using near-field microscopy. Surface & Coatings Technology 212:134–144
28. P. Salehikahrizsangi, F. Karimzadeh, M.H. Enayati, M.H. Abbasi, Investigation of the effects of grain size and nano-sized reinforcements on Tribological properties of Ti6Al4V alloy, Wear 305 (2013)51–57
29. Juan J. de Damborenea, Maria Aparecida Larosa, Maria Angeles Arenas, Juan Manuel Hernández-Lopez, André Luiz Jardini, Maria Clara F. Ierardi, Cecília A.C. Zavaglia, Rubens Maciel Filho, Ana Conde, Functionalization of Ti6Al4V scaffolds produced by direct metal laser for biomedical applications, Materials & Design 83 (2015) 6–13
30. Klenam DEP, Chown LH, Papo MJ, Cornish LA Characterization of railway stock axle produced from medium-carbon steel, advanced metals initiative nuclear materials development network conference 2015. The Southern African Institute of Mining and Metallurgy
31. Babatunde Abiodun Obadele, Anthony Andrews, Peter Apata Olubambi, Mathew T Mathew, Sisa Pityana, Effect of ZrO_2 addition on the dry sliding wear behavior of laser clad Ti6Al4V alloy 2015, Wear, 328, 295–300.
32. Mountford, J.A., 2002. Titanium-properties, advantages and applications solving the corrosion problems in marine service. NACE International.